Inorganic Chemistry

Article

pubs.acs.org/IC

Electronic Structures of Octahedral Ni(II) Complexes with "Click" Derived Triazole Ligands: A Combined Structural, Magnetometric, Spectroscopic, and Theoretical Study

David Schweinfurth,[±] J. Krzystek,*[,∫] Igor Schapiro,[§] Serhiy Demeshko,[∥] Johannes Klein,[ζ] Joshua Telser,*[,#] Andrew Ozarowski,[∫] Cheng-Yong Su,[¶] Franc Meyer,[∥] Mihail Atanasov,*[,§,$] Frank Neese,*[,§] and Biprajit Sarkar*[,±]

[±]Institut für Chemie und Biochemie, Freie Universität Berlin, Fabeckstraße 34-36, D-14195 Berlin, Germany

[∫]National High Magnetic Field Laboratory, Florida State University, Tallahassee, Florida 32310, United States

[§]Max Planck Institute for Chemical Energy Conversion, Stiftstraße 34-36, D-45470 Mülheim an der Ruhr, Germany

[∥]Institut für Anorganische Chemie, Georg-August Universität Göttingen, Tammanstraße 4, D-37077 Göttingen, Germany

[ζ]Institut für Anorganische Chemie, Universität Stuttgart, Pfaffenwaldring 55, D-70569 Stuttgart, Germany

[#]Department of Biological, Chemical and Physical Sciences, Roosevelt University, Chicago, Illinois 60605, United States

[¶]Lehn Institute of Functional Materials, School of Chemistry and Chemical Engineering, Sun Yat-Sen University, Guangzhou 510275, China

[$]Institute of General and Inorganic Chemistry, Bulgarian Academy of Sciences, 1113 Sofia, Bulgaria

Supporting Information

ABSTRACT: The coordination complexes of Ni(II) with the tripodal ligands tpta (tris[(1-phenyl-*1H*-1,2,3-triazol-4-yl)-methyl]amine), tbta ([(1-benzyl-*1H*-1,2,3-triazol-4-yl)methyl]-amine), and tdta (tris[(1-(2,6-diisopropyl-phenyl)-*1H*-1,2,3-triazol-4-yl)methyl]amine) and the bidentate ligand pyta (1-(2,6-diisopropylphenyl)-4-(2-pyridyl)-1,2,3-triazole), [Ni-(tpta)$_2$](BF$_4$)$_2$ (**1**), [Ni(tbta)$_2$](BF$_4$)$_2$ (**2**), [Ni(tdta)$_2$](BF$_4$)$_2$ (**3**), and [Ni(pyta)$_3$](BF$_4$)$_2$ (**4**), were synthesized from Ni(BF$_4$)$_2$·6H$_2$O and the corresponding ligands. Complexes **2** and **4** were also characterized structurally using X-ray diffraction and magnetically via susceptibility measurements. Structural characterization of **2** that contains the potentially tetradentate, tripodal tbta ligand revealed that the Ni(II) center in that complex is in a distorted octahedral environment, being surrounded by two of the tripodal ligands. Each of those ligands coordinate to the Ni(II) center through the central amine nitrogen atom and two of the triazole nitrogen donors; the Ni−N(amine) distances being longer than Ni−N(triazole) distances. In case of **4**, three of the bidentate ligands pyta bind to the Ni(II) center with the binding of the triazole nitrogen atoms being stronger than those of the pyridine. Temperature dependent susceptibility measurements on **2** and **4** revealed a room temperature $\chi_M T$ value of 1.18 and 1.20 cm^3 K mol^{-1}, respectively, indicative of S = 1 systems. High-frequency and -field EPR (HFEPR) measurements were performed on all the complexes to accurately determine their g-tensors and the all-important zero-field splitting (zfs) parameters D and E. Interpretation of the optical d−d absorption spectra using ligand field theory revealed the B and Dq values for these complexes. Quantum chemical calculations based on the X-ray and DFT optimized geometries and their ligand field analysis have been used to characterize the metal−ligand bonding and its influence on the magnitude and sign of the zfs parameters. This is the first time that such extensive HFEPR, LFT, and advanced computational studies are being reported on a series of mononuclear, distorted octahedral Ni(II) complexes containing different kinds of nitrogen donating ligands in the same complex.

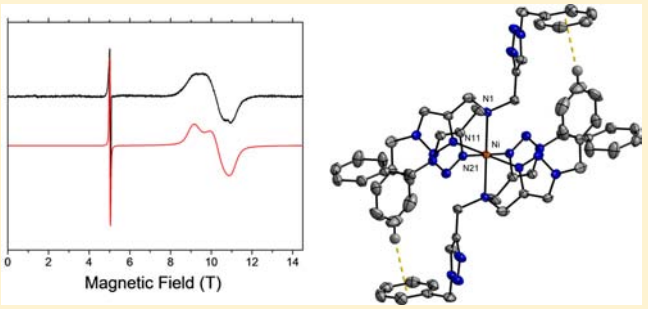

INTRODUCTION

The Cu(I) catalyzed cycloaddition reaction between azides and alkynes, a so-called "click" reaction, has established itself as an extremely powerful synthetic tool in organic chemistry.[1] Coordination chemists have taken advantage of this highly appealing reaction to design ligands for synthesizing a variety of metal complexes.[2] Several groups have undertaken projects of screening such metal complexes in various fields such as electron transfer,[3] photochemistry,[4] magnetism,[5] antitumor agents,[6] supramolecular chemistry,[7] and catalysis.[8] We have been utilizing metal complexes of "click" derived ligands for

Received: November 29, 2012
Published: May 23, 2013

   dx.doi.org/10.1021/ic3026123 | *Inorg. Chem.* 2013, 52, 6880−6892

understanding their fundamental properties and a variety of applications.[9] One field that is our focus at the moment is the magnetic properties of complexes of these ligands with 3d metal centers. We have thus shown that Co(II) complexes of tripodal triazole ligands can undergo temperature dependent spin crossover.[10a] Recently, we have reported on the catalytic poly- and oligomerization reactions with Fe(II), Co(II), and Ni(II) complexes of tripodal[10b] as well as bidentate[10c] "click" derived triazole ligands and have investigated their geometric and electronic structures.

Synthesizing new kinds of metal complexes and the complete understanding of their geometric and electronic structures is an all important goal in coordination chemistry. It is only through the development of innovative synthetic tools, as well as the structural understanding of metal complexes, that a rational basis for their application in various fields of chemistry can be achieved. High-frequency and -field electron paramagnetic resonance (HFEPR) spectroscopy has established itself as an extremely powerful tool for elucidating the electronic structures of metal complexes that are not amenable to conventional EPR techniques.[11] Traditionally, paramagnetic metal complexes containing more than one unpaired electron such as mononuclear tetrahedral or octahedral Ni(II) complexes have been investigated by magnetometry.[12] In these complexes the operation of zero-field splitting (zfs) often shifts the resonances outside the window available in standard EPR measurements.[13] Thus this type of complexes has been investigated with HFEPR spectroscopy, including model complexes for Ni-containing enzymes.[14] Octahedral Ni(II) complexes (S = 1) with N_4O_2,[14h,k,15d] N_3O_3,[14l] and N_2O_4[14i] donor sets have been subjected to such investigations. Very recently HFEPR studies have been reported also on Ni(II) complexes with a O_4E_2 (E = S or Se) donor set.[14m] To the best of our knowledge, reports on HFEPR spectroscopy on mononuclear Ni(II) complexes containing a N_6 coordination sphere are restricted to homoleptic complexes (where all six N donors are identical) and such reports number only a few.[14a,c]

Ligand field theory (LFT) has been broadly used as a tool to interpret spectral and magnetic phenomena in extended solids and molecular complexes of transition metals. Nowadays this model has been widely supplemented by advanced first principle density functional theory (DFT) and *ab initio* multireference electronic structure theory. In particular the latter theory was successfully applied to predict and interpret electronic multiplet structures and zfs tensors of transition metal 3d-complexes of unprecedented size using a well documented computational protocol as implemented in the program ORCA.[15] A one-to-one mapping procedure of the general nonadditive ligand field parametrization using *ab initio* wave functions allows to extract ligand field parameters from state average complete active space self consistent field (SA-CASSCF)[16] wave functions and from N-electron valence second order perturbation theory (NEVPT2).[17]

Herein we present the synthesis of four new complexes of Ni(II) with the tripodal ligands tpta (tris[(1-phenyl-*1H*-1,2,3-triazol-4-yl)methyl]amine), tbta ([(1-benzyl-*1H*-1,2,3-triazol-4-yl)methyl]amine), and tdta (tris[(1-(2,6-diisopropyl-phenyl)-*1H*-1,2,3-triazol-4-yl)methyl]amine) and the bidentate ligand pyta (1-(2,6-diisopropylphenyl)-4-(2-pyridyl)-1,2,3-triazole)), $[Ni(tpta)_2](BF_4)_2$ (**1**), $[Ni(tbta)_2](BF_4)_2$ (**2**), $[Ni(tdta)_2](BF_4)_2$ (**3**), and $[Ni(pyta)_3](BF_4)_2$ (**4**), from $Ni(BF_4)_2{\cdot}6H_2O$ and the corresponding ligands. The donor sets in these complexes can be described as trans-$N_4N'_2$ (in **1**–**3**) and meridional-$N_3N'_3$ (in **4**). Single crystal X-ray diffraction studies are presented on representative complexes **2** and **4** to determine the structural features and bonding anisotropies around the metal centers. SQUID magnetometric measurements are presented for the same two complexes to gather information about the bulk magnetic properties of the substances. HFEPR studies on these open shell S = 1 systems are reported, and spin Hamiltonian parameters are determined by that method. Ligand field theory is used to gain information about B and Dq parameters from the energies of the observed d–d transitions. Quantum chemical calculations and their ligand field (angular overlap model) analysis are used to gain insight into the origin of the metal–ligand bonding and its effect on the zfs in these complexes.

RESULTS AND DISCUSSION

Synthesis and Characterization. The ligands tbta and tpta were synthesized by reported methods[18] (Figure 1), and

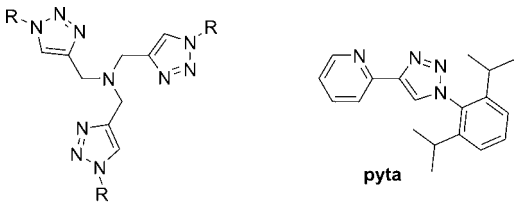

tpta; R = phenyl
tbta; R = benzyl
tdta; R = 2,6-diisopropylphenyl

Figure 1. Ligands used in this work.

the new ligands tdta and pyta were synthesized by a modified Cu(I) catalyzed "click" protocol. The modifications were undertaken to simplify the purification steps for this ligand (see Experimental Section).

The metal complexes were synthesized by reaction of $Ni(BF_4)_2{\cdot}6H_2O$ with the respective ligands for 1 h under reflux (see Experimental Section). Cooling of the reaction mixture to room temperature and filtration delivered good product yields after recrystallization. The purity of the complexes and their composition was verified by using elemental analysis and mass spectrometry (peaks corresponding to m/z values of $[M]^{2+}$ ions were observed (see Experimental Section)).

X-ray Diffraction Studies. Single crystals of **2** and **4** suitable for X-ray diffraction studies were grown by slow diffusion of diethyl ether into acetonitrile and ethanol solutions, respectively, at ambient temperatures. The complexes **2** and **4** crystallize in the triclinic $P\bar{1}$ and monoclinic $C2/c$ space groups, respectively (Table 1). In both **2** and **4**, the Ni(II) center is in a distorted octahedral environment, coordinated in the case of **2** by four triazole (N^{ta}) and two trans amine (N^{am}) nitrogen donors (trans-$N^{ta}_4N^{am}_2$ coordination mode, Figure 2) and in the case of **4** by pyridine (N^{py}) and triazole N-donors in a meridional arrangement (mer-N^{ta}_3, N^{py}_3, Figure 3).

In the centrosymmetric complex with the tripodal ligand tbta, **2**, the nickel center is coordinated by each tbta ligand through the nitrogen atoms N11 and N21 of two 1,2,3-triazole rings and the central amine nitrogen donors (N1), while the third triazole ring of each tbta ligand remains uncoordinated (Figure 2). The four nitrogen donors from the triazole rings thus make up the equatorial coordination at the nickel center

dx.doi.org/10.1021/ic3026123 | Inorg. Chem. 2013, 52, 6880–6892

Table 1. Crystallographic Data for 2 and 4

	2	4
formula	$C_{60}H_{60}B_2F_8N_{20}Ni$	$C_{57}H_{66}B_2F_8N_{12}Ni$
M_r	1293.61	1151.55
crystal system	triclinic	Monoclinic
space group	$P\bar{1}$	$C2/c$
a (Å)	10.171(1)	43.564(5)
b (Å)	11.408(3)	15.497(2)
c (Å)	13.979(3)	18.910(2)
α (deg)	93.79(2)	90
β (deg)	105.24(1)	105.320(7)
γ (deg)	94.67(1)	90
V (Å^3)	1553.2(6)	12313(2)
Z	1	8
D_{calc} (g cm^{-3})	1.383	1.242
T (K)	173(2)	100(2)
μ (mm^{-1})	0.394	0.385
Mo Kα (nm)	0.71073	0.71073
F(000)	670	4816
meas/ indep refl	6435/6077	29659/10743
obsvd [$I > 2\sigma(I)$] refl	4599	5060
R(int)	0.0399	0.1207
R[$F^2 > 2\sigma(F^2)$]	0.0390	0.0898
wR (F^2)	0.1032	0.2426
S	0.863	1.091
$\Delta\rho_{max}$, $\Delta\rho_{min}$ (e Å^{-3})	0.329, −0.529	1.150, −0.522

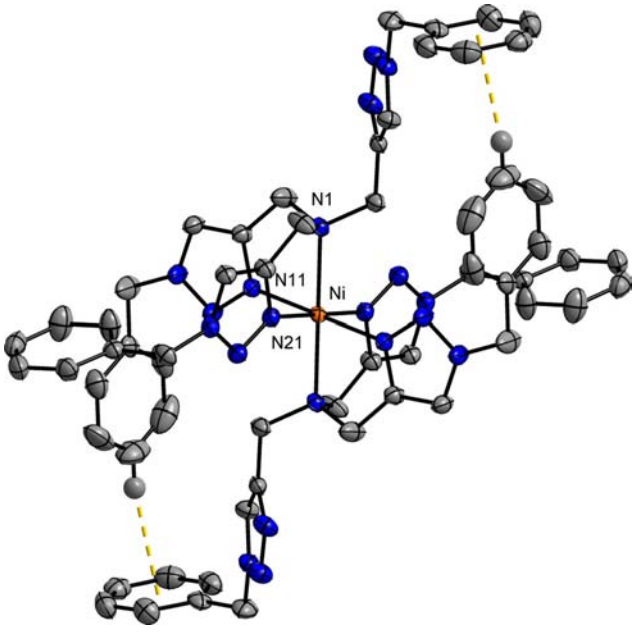

Figure 2. ORTEP plot of **2**. The BF_4^- ions are left out for clarity. Ellipsoids are drawn at 50% probability.

with Ni−N^{ta} distances of 2.040(2) and 2.071(2) Å (Table 2). In contrast, the Ni−N^{am} distance is much longer with 2.242(2) Å. As will be shown by LF analysis (vide infra), the amine nitrogen atoms are poorer donors than the triazole nitrogen atoms, and this is reflected in the larger Ni−N^{am} distances compared to the Ni−N^{ta} distances. DFT geometry optimization using a polarizable continuum model (COSMO) reproduces reasonably well the X-ray geometries (see Table 2). In addition to the bond length anisotropy, there is a significant angular distortion of the average value of the axial−equatorial angle,

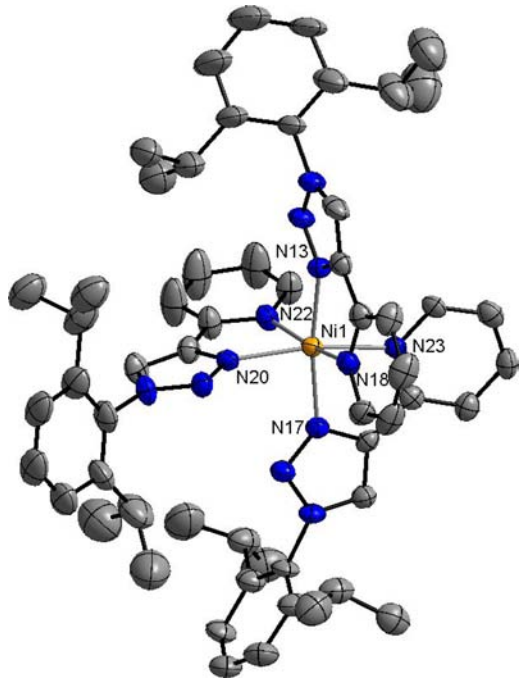

Figure 3. ORTEP plot of **4**. The BF_4^- ions are left out for clarity. Ellipsoids are drawn at 50% probability.

$\angle N^{am}NiN^{ta}$ (α, distortion denoted by $\delta\alpha$) from 90° (see Table 2). These differences in bond lengths and bond angles thus introduce bonding strain into the structure and reduce the symmetry around the Ni(II) from O_h to C_i. As will be shown this has a strong impact on the magnetic and spectral behavior.

The benzyl substituents of the uncoordinated 1,2,3-triazole rings of the tbta ligands participate in strong intramolecular C−H···π interactions with the benzyl substituents of a coordinated triazole ring (Figure 2). The distance between the C−H proton of one benzyl ring and the center of the phenyl ring of the other benzyl group is 2.7271(7) Å. The formation of such strong noncovalent interactions within the second coordination sphere of the metal center is a trademark of the tbta ligand in its bis(ligand)-complexes. We have recently shown that these noncovalent interactions are responsible for magnetic bistability in Co(II) complexes of tbta and will show here that these interactions affect the sign of the zero-field splitting.[10a]

Despite several attempts, we were unable to produce suitable crystals of complex **1** with BF_4^- as counteranion. Attempts at crystallizing a corresponding $[Ni(tpta)_2](ClO_4)_2$ analog (**1′**) were somewhat successful, but the quality of the X-ray diffraction data is not good enough to provide accurate bond lengths in that complex. To this end, DFT geometry optimizations were carried out on the entire **1**−**4** series (see Table 2 for a list of relevant Ni−N bond distances and N−Ni−N bond angles). The coordination geometry of **1** is very close to that of **2**; similar to **2**, the nickel center in **1′** is also coordinated through triazole nitrogen atoms in the equatorial plane and through amine nitrogen atoms in the axial direction. One triazole ring from each tpta ligand remains uncoordinated in **1′**, just as is the case of **2** with tbta. Thus the Ni(II) center in **1′** is observed (and also computed) to have the lowest symmetry (C_1). Furthermore, the direct phenyl substituents of tpta are unlikely to form C−H···π interactions of the kind discussed above for **2**, where the more flexible benzyl groups make such interactions possible.

dx.doi.org/10.1021/ic3026123 | Inorg. Chem. 2013, 52, 6880−6892

Table 2. Selected Bond Lengths (in Å) and Equatorial−Axial Angles α and $\delta\alpha$ (in deg.) for Complexes 2 and 4 (from X-ray Data) and from DFT Geometry Optimizations (for 1 to 4)

	1	2		3		4	
structural parameter	DFT	exp	DFT	DFT	structural parameter	exp	DFT
Ni−N^{am}(ax)	2.204	2.242(2)	2.224	2.237	Ni−N^{ta}(+z)	2.021(5)	2.034
Ni−N^{ta}(eq)	2.209	2.242(2)	2.224	2.236	Ni−N^{ta}(−z)	2.033(5)	2.040
	2.027	2.040(2)	2.019	2.072	Ni−N^{ta}(+x)	2.068(5)	2.059
	2.091	2.040(2)	2.019	2.041	Ni−N^{py}(−x)	2.111(5)	2.083
	2.050	2.071(2)	2.094	2.068	Ni−N^{py}(+y)	2.070(6)	2.088
	2.066	2.071(2)	2.094	2.076	Ni−N^{py}(−y)	2.101(6)	2.115
Ni−N^{ta}(eq) average	2.058	2.056	2.056	2.064	Ni−$N^{ta,py}$(eq) average	2.088	2.086
α_{av}	90.1	90.0	90.0	90.0		90.1	90.1
$\delta\alpha$	−12.0	−9.7	−10.5	−13.1		−11.1	−10.8
	+13.8	+9.4	+10.5	13.3		+7.8	+8.3

Similar to complex **1** we could not obtain single crystals of **3** appropriate for X-ray diffraction. DFT optimizations of this complex and the comparison of bond lengths and angles (Table 2) show that the coordination of Ni(II) in **3** is very similar to **1** and **2**. This is also supported by the zfs tensor parameters from analysis of the HFEPR (vide infra).

The nickel center in complex **4** is coordinated by three of the bidentate pyridyl-triazole ligands, pyta (Figure 3). The three triazole N donors take up meridional positions around the nickel centers, as do the pyridyl N donors.

Unlike **2** and similar to **1**, the Ni(II) complex in **4** does not contain a center of symmetry. The three principal bonding axes of the octahedron in **4** are also all different. This is a consequence of the meridional coordination mentioned above, together with the bis-chelating nature of the pyta ligand. Thus one of the bonding axis has two triazole nitrogens *trans* to each other (N13−Ni1−N17, Figure 3), the second one has two pyridine nitrogens trans to each other (N18−Ni1−N22), and the final one has a pyridine and a triazole nitrogen trans to each other (N20−Ni1−N23). On average the Ni−N^{ta} bond lengths are shorter than the Ni−N^{py} bond lengths (Table 2). Similar observations have been made by us and others for metal complexes with related pyridyl-triazole ligands.[7a,9a,b] As supported by the ligand field analysis of the *ab initio* results, this trend reflects the slightly larger donor ability of the triazole nitrogen atom as compared to the pyridine nitrogen atom. Thus the three different bonding axes make the coordination around the nickel center in **4** less anisotropic than that in **1**−**3**. The distortion around the Ni(II) center in **4** is also apparent from the angles between the metal center and the donor atoms; for instance, the N20−Ni1−N22 angle is 78.8(2)°.

Magnetic Properties. The magnetic susceptibility of **2** and **4** was measured as a function of temperature between 2 and 295 K. Complex **2** was chosen as a representative for the series of complexes with the tripodal ligands, and additionally the magnetic properties of **4**, which contains bidentate ligands, were also investigated. The $\chi_M T$ versus T plots are shown in Figure 4.

The room temperature $\chi_M T$ values for **2** and **4** are 1.18 and 1.20 cm^3 K mol^{-1}, respectively. The magnetic susceptibility for both complexes remains constant down to ca. 8 K. Within this range both complexes follow the Curie−Weiss behavior as can be expected for an octahedral Ni(II) center isolated from its immediate environment through bulky ligands. Below 8 K, the $\chi_M T$ values for both the complexes show a sharp drop, which is a consequence of zfs. Fitting the spin Hamiltonian parameters that included terms for axial zero-field and isotropic Zeeman

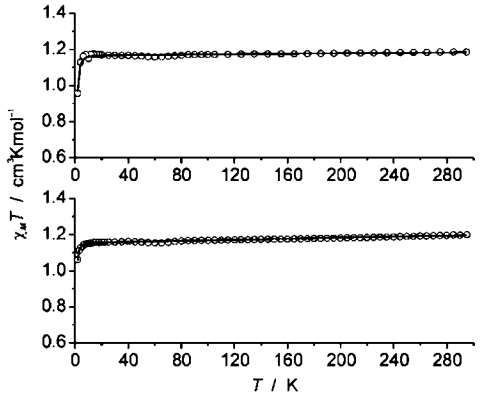

Figure 4. Plots of $\chi_M T$ versus T for **2** (top) and **4** (bottom) at 0.5 T. The solid lines represent the calculated curve fits (see text for appropriate parameters).

splitting (see Experimental Section) delivered $|D|$ values larger for **2** (2.3 cm^{-1}) compared to **4** (1.5 cm^{-1}).

Additionally, the fits indicated important spin−orbit contributions to the spin-only value of g = 2.00 (2.16 and 2.15 for **2** and **4**, respectively). The data thus reveal the significant magnetic anisotropy in complexes **2** and **4**. However, the magnitude and sign of D obtained from such powder measurements are not reliable. This is not only a well-known problem in magnetometry, as has been recently pointed out in a work dealing with Ni(II) complexes,[14m] but also a possible influence of other effects such as weak intermolecular interactions or measurement artifacts at low temperatures due to the orientation of the microcrystals in the magnetic field. Attempts to include a rhombic zfs parameter E in magnetic data analysis did not lead to any improvement of the fit quality. The more reliable data extracted out of detailed HFEPR measurements are discussed in the next section.

HFEPR Spectroscopy. Complexes **1**−**4** delivered HFEPR spectra characteristic for an S = 1 spin state. The quality of those spectra, however, varied from one complex to another. In general the observed line widths were very large; single-crystal line widths assumed in simulations were typically of the order of 200 mT for the allowed ($\Delta M_S = \pm 1$) transitions, and 50 − 70 mT for the "half-field" ($\Delta M_S = \pm 2$) transition. Figure 5 shows the collection of spectra acquired at 5 K and at approximately the same frequency (295 − 305 GHz). The experimental spectra are accompanied by powder-pattern simulations, using S = 1 spin Hamiltonian parameters obtained from multifrequency experiments (see below). Only in the case

dx.doi.org/10.1021/ic3026123 | Inorg. Chem. 2013, 52, 6880−6892

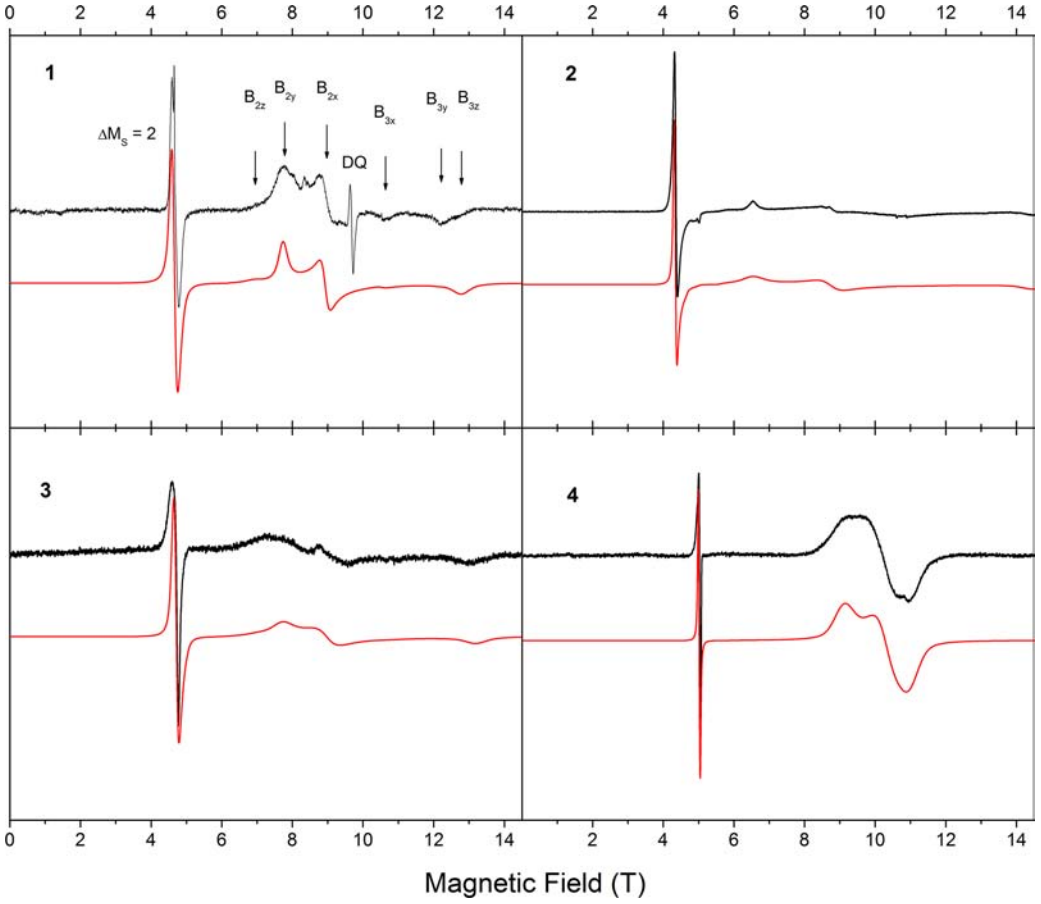

Figure 5. Experimental spectra (black traces) of complex **1** at 295.2 GHz and **2**–**4** at 304.8 GHz, both at 5 K. The red traces are simulations assuming $S = 1$ spin Hamiltonian parameters as in Table 3 for all complexes except **3**, for which they were as follows: $D = +3.08$ cm^{-1}, $E = +0.50$ cm^{-1}, $g = [2.20, 2.15, 2.15]$. Single-crystal line widths assumed in the simulations were [100, 100, 200 mT] for $\Delta M_S = 1$ transitions, 70 mT for $\Delta M_S = 2$ transitions in complex **1**; isotropic 200 mT for $\Delta M_S = 1$ transition, 50 mT for $\Delta M_S = 2$ transitions in complexes **2** and **3**; isotropic 250 mT for $\Delta M_S = 1$ transitions, 50 mT for $\Delta M_S = 2$ transition in **4**. The particular turning points are labeled for complex **1**. DQ stands for a double-quantum transition that is not simulated.

of complex **3** we needed to "tweak" the parameters a bit to achieve a better agreement between experiment and simulation for that particular frequency. Single-frequency simulations proved that in each case except complex **4**, the zfs parameters are positive (simulations for negative parameters are not shown). In the case of **4**, the rhombicity of its zfs tensor makes the sign of little relevance; yet the simulations using negative values were slightly better than the positive ones.

Because of well-known problems with torquing in high magnetic fields and consequent distortions of the ideal powder patterns, we chose to extract the spin Hamiltonian parameters from a multifrequency 2-D map of resonances for each complex rather than from single-frequency spectra, according to the principle of tunable-frequency EPR.[19] Figure 6 shows a collection of such maps for each of the investigated complexes.

The spin Hamiltonian parameters fitted to the 2-D maps as in Figure 6 are collected in Table 3. From those, one can see that complexes **1** and **3** have basically identical parameters with D ca. (positive) 3 cm^{-1}, while complex **2** has zfs larger by about 50%, and complex **4** is smaller by a factor of 3. These findings will be analyzed below. The g factors remain in the same range of 2.12–2.18 for all the compounds, and their anisotropy is rather small. Note that although the D values determined by magnetometry for **2** and **4** differ from those determined by HFEPR by 50%, the isotropic g value determined by magnetometry for each complex agrees perfectly with the average of the anisotropic g values determined by HFEPR.

Ligand Field Theory. Complexes **1**, **2**, and **3** have sufficiently similar electronic absorption spectra such that there is no point in attempting individual fits. Rather, we use the following consensus values for the three spin-allowed transitions for octahedral Ni(II) (see Figure 7 and Supporting Information) in these complexes taken together: $^3A_{2g}(^3F) \rightarrow {}^3T_{2g}$ at 11000 ± 100 cm^{-1}, $^3A_{2g}(^3F) \rightarrow {}^3T_{1g}(^3F)$ at 18250 ± 100 cm^{-1}, and, $^3A_{2g}(^3F) \rightarrow {}^3T_{1g}(^3P)$ at 28900 ± 100 cm^{-1}. Fitting ligand-field parameters as defined by Ballhausen[20] to these transitions gives $B = 875$ cm^{-1}, $Dq = 1130$ cm^{-1}. Complex **4** similarly yielded $B = 850$ cm^{-1}, $Dq = 1160$ cm^{-1}. These values are in good agreement with those determined for an extensive series of tetraazamacrocyclic complexes of Ni(II) with a variety of axial ligands, as reported by Busch and co-workers.[21] For example, Ni([14]aneN4)(NCS)$_2$, a complex with a similar N_4N_2 donor set, gave $B = 860$ cm^{-1}, $Dq = 1418$ cm^{-1}.[21b] The electronic absorption data do not permit extraction of parameters characterizing the axial distortion of the ligand field (Ds, Dt), in contrast to the studies by Busch and co-workers. For there to be zfs, such distortion must be present and it is suggested by the different Ni–N bond lengths (2.04, 2.07, and 2.24 Å in **2**). Inclusion of small tetragonal distortion that is consistent with the electronic transitions with $\zeta = 540$

dx.doi.org/10.1021/ic3026123 | Inorg. Chem. 2013, 52, 6880–6892

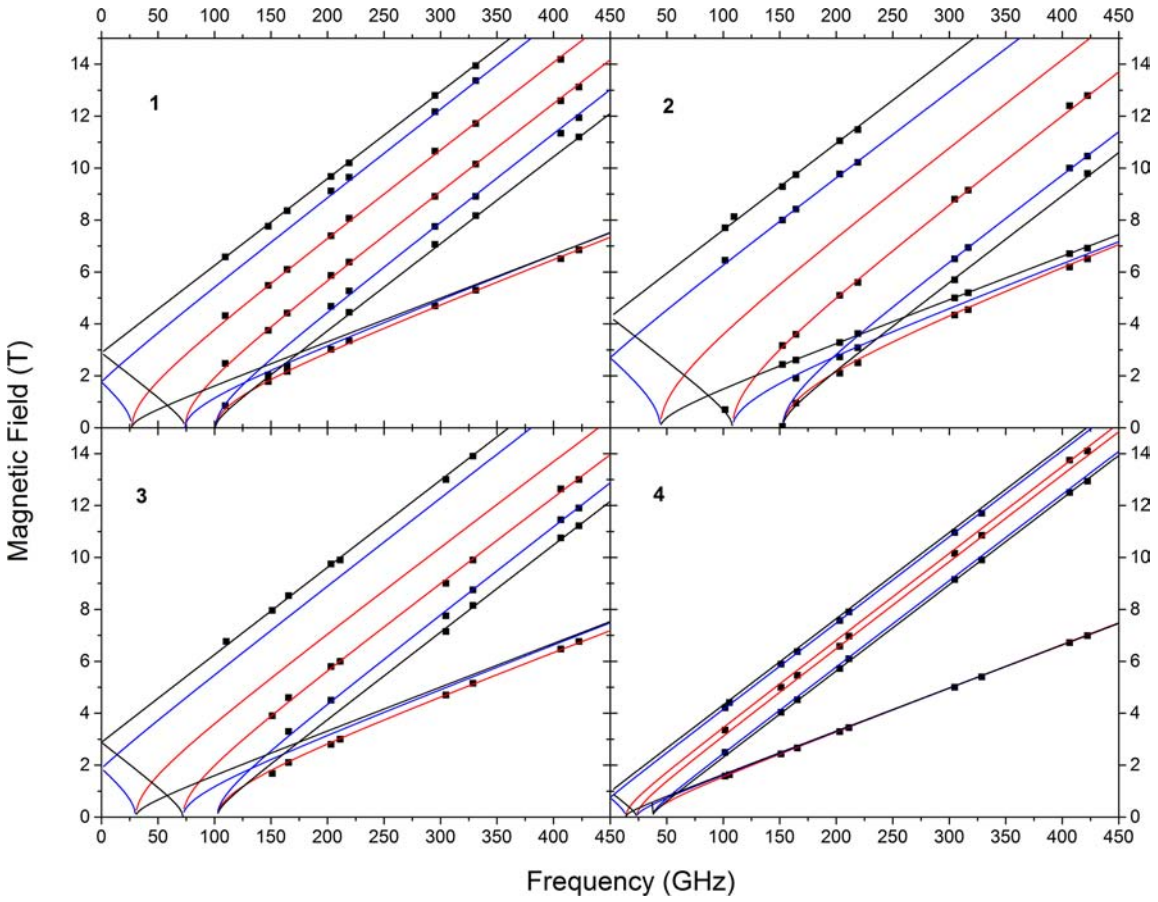

Figure 6. Two-dimensional maps of turning points in the HFEPR spectra of the investigated complexes. Squares are experimental data at 5 K; lines were drawn using the spin Hamiltonian parameters as in Table 3. Red lines represent $B_0//x$ turning points, blue lines represent $B_0//y$, and black lines represent $B_0//z$ resonances.

Table 3. Spin Hamiltonian Parameters of the Investigated Complexes As Determined by HFEPR

complex	D (cm^{-1})	E (cm^{-1})	E/D	g_x	g_y	g_z
1	+2.92(2)	+0.45(1)	0.15	2.135(5)	2.108(6)	2.138(6)
2[a]	+4.35(2)	+0.738(4)	0.17	2.143(7)	2.178(6)	2.150(6)
3	+2.91(3)	+0.50(3)	0.17	2.18(1)	2.120(15)	2.130(6)
4[b]	±1.01(3)	±0.23(1)	0.23	2.140(2)	2.152(7)	2.152(6)

[a]Variable temperature magnetic susceptibility for **2** gave $|D| = 2.3$ cm^{-1} and $g_{iso} = 2.16$, which agrees exactly with the average g value from HFEPR. [b]Variable temperature magnetic susceptibility for **4** gave $|D| = 1.5$ cm^{-1} and $g_{iso} = 2.15$, which agrees exactly with the average g value from HFEPR.

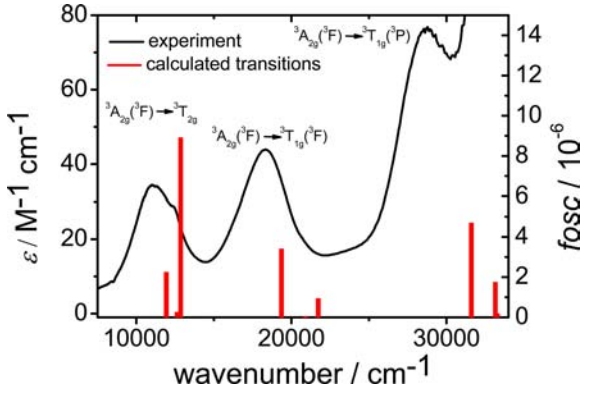

Figure 7. Absorption spectrum of **1** in CH_3CN together with calculated (NEVPT2) transitions (red sticks). The bands are identified based on the complexes' idealized O_h point group symmetry.

cm^{-1} (~80% of the free-ion value)[22] leads to $D \approx 0.8$ cm^{-1}, much less than the experimental value for complexes **1**–**3**, but comparable to that seen for complex **4**. This approach does not include spin–spin coupling (SSC), which is expected to yield only negligible contributions for $S = 1$ states. A more detailed analysis of the electronic absorption spectra was performed by quantum chemical calculations and their ligand field analysis as discussed below.

Quantum Chemical Calculations. To gain a better insight into the origin of zfs in the complexes under investigation and for better understanding their absorption spectra, elaborate *ab initio* calculations at the NEVPT2 level of theory[17,15] were performed.

As was recently shown, *ab initio* calculations correlate well with the traditional LFT approach.[15] For this reason, the electronic transitions in the absorption spectra of **1**, **2**, and **4** were assigned on the basis of the NEVPT2 method. Correlated calculations on complex **3** were prohibited by its large size. A

dx.doi.org/10.1021/ic3026123 | Inorg. Chem. 2013, 52, 6880–6892

Table 4. Absorption Spectra of 1 in CH_3CN and Their Deconvolution Compared to Calculated Transitions with the NEVPT2 Method Based on the Optimized Geometry of 1

	experiment				NEVPT2	
transitions (in O_h)	maximum (cm^{-1})	ε (M^{-1} cm^{-1})	deconv (cm^{-1})	f_{osc} ($\times 10^{-6}$)[a]	energy (cm^{-1})	f_{osc} ($\times 10^{-9}$)[a]
$^3A_{2g}(^3F) \rightarrow {}^3T_{2g}$	11 200	34.0	8200	225	11 936	2251
			11 000	229	12 628	251
			11 700	253	12 856	8910
$^3A_{2g}(^3F) \rightarrow {}^3T_{1g}(^3F)$	18 400	43.8	17 700	426	19 357	3403
			18 700	72	20 922	56
			20 700	654	21 731	939
$^3A_{2g}(^3F) \rightarrow {}^3T_{1g}(^3P)$	28 700	76.5	28 800	1572	31 604	4693
					33 148	1745
					33286	183

[a]Listed numbers for the (dimensionless) oscillator strength f_{osc} have to be multiplied by the factors given in parentheses.

Table 5. Contributions to the Zero-Field Splitting Parameters (in cm^{-1}) from SA-CASSCF and NEVPT2 Calculations Using 14 Excited States (9 Triplets and 5 Singlets)[a]

			SA-CASSCF			NEVPT2		
compd	method	state	energy	D	E	energy	D	E
1	2nd PT	^3A	8350	25.2	15.7	11 559	18.2	5.2
		^3A	8879	11.7	−12.8	12 255	1.9	−4.3
		^3A	9467	−31.2	−1.1	12 612	−16.7	0.2
		^1A	26 060	−7.2	−6.8	27 104	−6.8	−5.2
		^1A	26 480	−6.6	6.4	27 730	−5.2	4.8
		^1A	27 247	13.6	0.0	28 523	11.8	0.1
		sum of all		+5.80	+1.26		+3.36	+0.74
	QDPT			+4.80	+1.06		+2.94	+0.66
	expt						+2.92(2)	+0.45(1)
2	2nd PT	^3A	8085	24.5	25.3	11 109	17.0	17.8
		^3A	8515	22.3	−23.7	11 672	14.9	−16.7
		^3A	9848	−38.9	0.1	13 091	−27.2	0.2
		^1A	25 849	−7.1	−7.2	26 724	−6.7	−6.9
		^1A	26 161	−6.8	6.9	27 198	−6.3	6.6
		^1A	27 521	13.4	−0.0	28 897	12.4	−0.0
		sum of all		+7.74	+1.25		+4.48	+0.75
	QDPT			+5.95	+1.20		+3.79	+0.66
	expt						+4.35(2)	+0.738(4)

[a]Optimized geometry of **1** and X-ray geometry of **2** were used.

full list of the energies of the spin-allowed d−d transitions of complexes **2** and **4** based on their X-ray and DFT geometry optimized structures for **1**, **2**, and **4** are listed in Table S3 (Supporting Information). The energies obtained from calculations based on optimized structures compare well with the ones based on the X-ray structure.

The reduction of symmetry leads to the splitting of the $^3T_{2g}$ and $^3T_{1g}$ states into three nondegenerate sublevels. In contrast, the experimental absorption spectra show only three main bands, which are due to overlapping absorption bands which can be resolved starting with the NEVPT2 excitation energies and refining their values by a fit to the experimental d−d absorption band profile. For further analysis the experimental absorption spectra were subjected to spectral deconvolution, allowing for a better comparison with the theoretical results.

Figure 7 shows the experimental absorption spectrum of **1** in CH_3CN (black trace) together with calculated transitions on the NEVPT2 level (red bars). Each of the three main bands could be fitted with three Gaussian distributions representing the three times three possible transitions with the sum of these distributions in excellent agreement with the experimental spectrum (SI, Figures S1−S3).

The absorption spectra of **1**, **2**, and **4** in acetonitrile were calculated on the SA-CASSCF/NEVPT2 level of theory including all of the possible 24 excited states (9 triplets and 15 singlets, which with the triplet ground state result in a total of 45 microstates of d^8). In Table 4, the energies dominated by the triplet states for **1** are shown; energies for **2** and **4** can be found in the Supporting Information (Table S1). All triplet states contribute to the absorption spectrum due to spin-allowed transitions. Spin-forbidden transitions have not been observed.

The theoretical investigation helps to clarify the experimental results: Even though the reduction of symmetry leads to splitting of a given state, there is always one out of three transitions that has much stronger oscillator strength (f_{osc}) than the others. For compound **1**, the three calculated transitions with the major oscillator strength show up at 12856, 19357, and 31604 cm^{-1}, which compares reasonably well with the experimental maxima at 11200, 18400, and 28700 cm^{-1} respectively. Therefore, in the experimental spectrum only

dx.doi.org/10.1021/ic3026123 | Inorg. Chem. 2013, 52, 6880−6892

three main bands are observed, despite considerable axial elongation. However, these experimental bands are relatively broad and, in the case of the lowest energy band, somewhat distorted in line shape. Thus, spectral deconvolution helps to uncover the underlying weaker transitions, which compare well with the calculated ones (Figures S1−S3 in the Supporting Information).

After thorough evaluation of the absorption spectra, *ab initio* methods were used for examination of the zfs parameters. In a first attempt, all excited states (9 triplets and 15 singlets) were included in the calculation (see Supporting Information, Table S2). In a recent series of papers,[23] a computational strategy was presented wherein not all excited states were included in the state-averaged CASSCF wave function. This has significantly improved the description of the orbitals of the zero order wave function since not all roots contribute to the zfs phenomenon. Even though the other states do not contribute to the zfs, they were equally weighted with roots that contribute. Those were mainly the first set of excited triplet states, ^{3}A, and a set of excited singlet states, ^{1}A.[14m] This strategy leads to a less biased description, hence the number of excited states was reduced from 15 to 5, including only the states important for the zfs.

In Table 5, only the states with significant contributions to the zfs are shown. Compound **4** is not discussed because of the rhombicity of the system. The major contribution to the zfs comes from the excited triplet states stemming from the $^3T_{2g}$ octahedral term, whereas the excited singlet states contribute only in a minor way, as revealed by second order perturbation theory (PT2). Comparing the SA-CASSCF and the NEVPT2 approaches, it can be seen in particular that, due to the dynamic electron correlation added by the NEVPT2 treatment, the excited triplet states shift to higher energies. As a result, the zfs parameters D and E are reduced almost by 50%, as zfs qualitatively is inversely proportional to excited state energies, which is an effect taking into account the covalency of the system. The final D values calculated by quasi degenerate perturbation theory (QDPT) are +2.94 and +3.79 cm^{-1} for **1** and **2**, respectively, which is in excellent agreement with the values determined by HFEPR (+2.92(2) and +4.35(2) cm^{-1}, respectively). Because QDPT considers all contributions to the zfs, it yields very accurate values, but in comparison to the PT2 approach, it does not allow to discuss the single contribution of the excited states to the total zfs.

These results clearly point to the necessity of NEVPT2 calculations on top of the CASSCF treatment to add dynamic correlation and thereby covalency. This multireference approach is applicable even for large molecules, like the complexes under investigation, thus showing the broad applicability of this methodology.

Ni(II)−Ligand Bonding as Revealed by a Ligand Field Analysis of the Ab Initio Results. A considerable insight into the nature of the metal ligand bond can be gained by deriving ligand field parameters from the rich database offered by CASSCF/NEVPT2 results (*ab initio* ligand field theory).[15a,c] Numerical values of the parameters of the ligand field given by the matrix elements of the symmetric 5 × 5 ligand field matrix of eq 1 and in addition, the Racah parameter B of d−d interelectronic repulsion have been computed from a best fit to the 10 × 10 matrix of the total of the 10 triplet states of Ni(II) in the considered complexes (for a detailed outline of the procedure for complex **4**, taken as an example, see Supporting Information.)

$$V = \begin{bmatrix} V_{xy,xy} & V_{yz,xy} & V_{z2,xy} & V_{xz,xy} & V_{x2-y2,xy} \\ V_{yz,xy} & V_{yz,yz} & V_{z2,yz} & V_{xz,yz} & V_{x2-y2,yz} \\ V_{z2,xy} & V_{z2,yz} & V_{z2,z2} & V_{xz,z2} & V_{x2-y2,z2} \\ V_{xz,xy} & V_{xz,yz} & V_{xz,z2} & V_{xz,xz} & V_{x2-y2,xz} \\ V_{x2-y2,xy} & V_{x2-y2,yz} & V_{x2-y2,z2} & V_{x2-y2,xz} & V_{x2-y2,x2-y2} \end{bmatrix} \quad (1)$$

Equation 1 represents the ligand field matrix in the most general form independent of any additive ligand field approximations (see Supporting Information eqs S8 and S10−S14 for numerical values of the matrix $\boldsymbol{V}$ for complexes **1**, **2**, and **4**). Diagonalization of the matrix in eq 1 yields ligand field orbital energies for complexes **1**, **2**, and **4** as depicted in Figure 8.

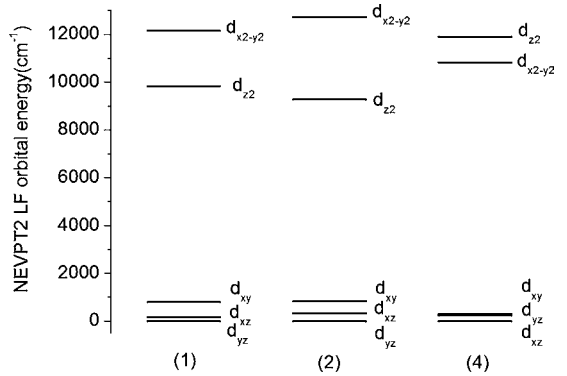

Figure 8. Metal based d-MO energies from *ab initio* ligand field analysis (AILFT) of NEVPT2 multireference electronic structure calculations for **1** (from the DFT optimized complex geometry) and for **2** and **4** (with geometries from X-ray data). Labeling of orbitals pertain to a coordinate system choice with the z, y, and x axes respectively oriented parallel to the trans N^{am}−N^{am}, N^{ta}−N^{ta}, and N^{ta}−N^{ta} bond directions in **1** and **2**, and the N^{ta}−N^{ta}, N^{py}−N^{py}, and N^{ta}−N^{py} bond directions in **4** (see also Table 2).

An energy order of d-MOs $d_{yz} \leq d_{xz} < d_{xy} < d_{z^2} < d_{x^2-y^2}$ (for **1** and **2**) and $d_{xz} \leq d_{yz} < d_{xy} < d_{x^2-y^2} < d_{z^2}$ (for **4**) results from *ab initio* LFT analysis. On the basis of the very small splitting of the d_{xz}, d_{yz}, and d_{xy} type orbitals we infer from this analysis that π Ni−N bonding is weak in all reported complexes. Correlated calculations on complex **3** were prohibited by its large size. However, on the basis of the very similar DFT optimized coordination geometries for **1**, **2**, and **3** (see Table 2) we can safely assume that bonding in **3** is similar to that in **1** and **2**, i.e., it is not significantly altered by more distant substituents. The very weak metal ligand π interactions reflected by the parameter e_π is consistent with the d_{xz}, d_{yz}, and d_{xy} orbitals being doubly occupied in the ground state configuration $t_{2g}^6 e_g^2$ of Ni(II). This compensates the energy stabilization due to Ni−N donor interactions and agrees with the weak Ni−N π-bonding inferred from analysis of d−d absorption and EPR spectra of Ni(II) complexes with similar N-donor ligands.[24] The large d_{z^2}−$d_{x^2-y^2}$ MO splitting features the distinctly weaker σ-antibonding character of the Ni(II)-N amine compared with the Ni−N triazole ligand. The resulting tetragonally elongated octahedral geometry is also reflected by the large and positive D values deduced from the HFEPR results (see Table 3). In contrast to

dx.doi.org/10.1021/ic3026123 | Inorg. Chem. 2013, 52, 6880−6892

Table 6. Ni−N AOM Parameters, the Racah Parameter *B*, and Zero-Field Splitting Parameters (in cm^{-1}) from a Best Fit of the AOM to Ab Initio NEVPT2 Results

complex	1	2		4	
	DFT opt	X-ray	DFT-opt	X-ray[b]	DFT-opt
e_σ^{py}				3706	3824
$e_{\pi s}^{py}$				−131	−200
e_σ^{ta}	4083	4131	4034	3859	3827
$e_{\pi s}^{ta}$	217	167	199	−276	−113
e_σ^{am}	3256	2802	3033		
B	1202	1200	1199	1212	1204
σ(AOM)[a]	393	421	454	282	269
$D(D_{exp})$	+2.30 (+2.92)	+3.23	−4.14 (+4.35)	e: $D_N{}^{ta}{}_N{}^{ta}$ = −0.98 (12°)	$D_N{}^{ta}{}_N{}^{ta}$ = −0.91 (18°); D_{exp} = ±1.00
$E(E_{exp})$	+0.87 (+0.45)	+0.76	−0.54 (+0.74)	m: $D_N{}^{py}{}_N{}^{py}$ = +0.02 (18°)	$D_N{}^{ta}{}_N{}^{py}$ = +0.28 (18°); E_{exp} = ±0.23
				h: $D_N{}^{ta}{}_N{}^{py}$ = +0.96 (12°)	$D_N{}^{py}{}_N{}^{py}$ = +0.64 (13°)

[a]Standard deviation between ligand field matrix elements from NEVPT2 calculations using DFT optimized (**1**, **2**, **3**) and X-ray (**2**, **4**) geometries and their respective AOM values calculated using the listed best fit AOM parameters. [b]The letters "e", "m", and "h" in the last row imply the directions of the easy, medium, and hard magnetic axis as identified by the computed signs of the main values of zfs tensor; the entries listed in parenthesis show the deviations (in deg) between the calculated "e", "m", and "h" directions and the corresponding $N^{ta}N^{ta}$, $N^{py}N^{py}$, and $N^{ta}N^{py}$ bond axes in **4**.

the coordination geometries of **1**, **2**, and **3**, the orbital energies of **4** reflect an almost homogeneous coordination environment. A much smaller $d_{x^2-y^2}$−d_{z^2} energy difference reflects the very close σ-antibonding properties of the two triazole and pyridine ligands with the triazole ligand acting as a slightly stronger σ-donor toward Ni(II). Based on the slightly compressed geometry ($d_{z^2} > d_{x^2-y^2}$) a negative sign of D would be expected. However, the additional angular distortions and the resulting very low (C_1) symmetry renders the computed (and also observed by HFEPR) zfs tensors almost entirely rhombic (see Tables 3 and 6). A quantification of the qualitative conclusions based on the ligand field MO diagram (Figure 8) is possible by an angular overlap model (AOM)[25,26] analysis of the *ab initio* LF matrices V (eq 1 and discussion in Supporting Information). This model is less general, but more appealing for chemists, although the AOM parametrization is not always unique. In standard applications of the AOM, up to four independent AOM parameters (deriving from energy differences due to complete C_1 low-symmetry splitting of the five d-orbitals) can be computed. However, focusing on complex **4**, six such parameters e_σ, $e_{\pi s}$ and $e_{\pi c}$, respectively denoting the σ-bonding, out-of-plane π-bonding, and in-plane π-bonding parameters for each of the two ligand types, the N-pyridine (py) and N-triazole (ta), result. Here we adopt a parametrization in which the in-plane π parameters, $e_{\pi c}$, for both ligand types have been set to zero, as there are no energetically favorable interactions of the N ligand orbitals in the plane, as these are involved in stronger bonds with the ligand framework atoms attached to them. To discern the effect of the out-of-plane parameter, $e_{\pi s}$, on the AOM matrix elements, we used a dummy atom attached to each N-ligand defining the (py) and (ta) ligand planes. Utilizing the exact geometry of complex **4** from the X-ray structure and from DFT geometry optimizations, AOM parameters from a least-squares fit to the V matrices were derived (Table 6, see a detailed outline of the procedure applied to this complex in Supporting Information). As seen by the rather small standard deviation (282 cm^{-1}, NEVPT2 results), the consistency of the fit is remarkable. From these results we can deduce that Ni−N bonding is dominated by Ni−N^{ta} and Ni−N^{py} σ-antibonding interactions with comparable values for the two ligands. In contrast, out-of-plane π-bonding reflected by the parameters $e_{\pi s}^{py}$ = −131 and $e_{\pi s}^{ta}$ = −276 cm^{-1} is of very small magnitude and negative, i.e., of the π-back bonding type. The very nearly octahedral ligand field of complex **4** is in agreement with its electronic spectrum which shows no resolved splitting of the transitions of the octahedral parent geometry (Figure S3). In agreement with this conclusion, D and E parameters resulting from the analysis of the HFEPR spectrum of **4** are considerably smaller than those for **1**−**3** (Tables 3 and 6).

AOM parameters deduced from NEVPT2 results for complex **4** have been compared with those resulting from CASSCF (accounting for static electron correlation, Table 7)

Table 7. AOM Parameters for 4 from LF Analysis of CASSCF and NEVPT2 Results

parameter	CASSCF (cm^{-1})	NEVPT2 (cm^{-1})
e_σ^{py}	3210	3706
$e_{\pi s}^{py}$	−121	−131
e_σ^{ta}	3379	3859
$e_{\pi s}^{ta}$	−246	−276

where the effect of the excited charge transfer states on the $3d^8$ multiplets of Ni(II) have been neglected. From this comparison we conclude that Ni−N covalence (charge transfer, dynamical correlation) yields important contributions to AOM parameters.

Complexes **1** and **2** present coordination spheres with two axial Ni−N^{am} in trans positions to each other (forming longer Ni−N^{am} bonds, 2.242 (in **2**) and 2.206 ± 0.003 Å (in **1**, average value) and four shorter Ni−N^{ta} bonds in equatorial positions (2.056 ± 0.015 Å (2) and 2.058 ± 0.033 Å (1)), respectively. The rather similar coordination environments of the two complexes give rise to similar multiplet energies. In Supporting Information (Table S2) we list their values from CASSCF and NEVPT2 calculations where electronic energy levels have been assigned using the O_h parent symmetry. However, the true, low symmetry is important as it leads to a splitting of the triplet cubic terms.

The NEVPT2 matrices for the DFT optimized structures of **1** and **2** and for the X-ray structure of **2** were further analyzed with the AOM adopting the following parametrization: the in-plane π-bonding parameters, $e_{\pi c}$, for the N^{ta} ligand was set to zero as in complex **4** and only σ-antibonding were taken into account in the case of N^{am}. For understanding the out-of-plane

dx.doi.org/10.1021/ic3026123 | Inorg. Chem. 2013, 52, 6880−6892

parameter $e_{\pi s}$, we used as for **4** a dummy atom attached to each of the N^{ta} ligand planes. Utilizing the exact geometry of **1** from the DFT geometry optimization and for **2** from the X-ray data we have adjusted the three AOM parameters e_{σ}^{am}, e_{σ}^{ta}, $e_{\pi s}^{ta}$ to the (over)complete set of elements of the matrices V_{NEVPT2} (Table 6). This leads us to the following values of these parameters: e_{σ}^{am} = 3256, e_{σ}^{ta} = 4083, $e_{\pi s}^{am}$ = 217 cm^{-1} (for **1**) and e_{σ}^{am} = 2802, e_{σ}^{ta} = 4131, $e_{\pi s}^{ta}$ = 167 cm^{-1} (for **2**). Reasonably small standard deviations between calculated AOM matrix elements, using these parameters and their original *ab initio* NEVPT2 values (393 cm^{-1} for **1** and 421 cm^{-1} for **2**, see Table 6) demonstrate the consistency of the fit and the adequacy of the parametrization scheme. From these results we can deduce, as for **4**, that Ni−N bonding in **1** and **2** is dominated by Ni−N^{ta} and Ni−N^{am} σ-antibonding interactions. However, σ-donation for N^{ta} is distinctly more pronounced as compared to N^{am}. This is also reflected in the shorter Ni−N bond distances for the latter ligand compared to the former.

Comments on Combined Experimental and Theoretical Results. The complexes **1**−**4** provide a unique opportunity of comparing six-coordinated Ni(II) complexes with two different types of substituted 1,2,3-triazole ligands; whereas the tripodal varieties in **1**−**3** contain a $N_4N'_2$ coordination around the Ni(II) center, **4** contains a $N_3N'_3$ donor set with the triazole N and pyridyl N taking up a meridional coordination. Structurally, **2** shows a pronounced axial elongation because of the weak amine donors of the tripodal ligands. This is also seen for **1′** (and hence for **1**) and is expected for **3**, for which we unfortunately could not generate appropriate single crystals. Complex **2** has unique, intramolecular weak interactions in its secondary coordination sphere because of the benzyl substituents of tbta. These interactions most likely contribute to the total ligand field stabilization energy, as has been shown by us recently for the related Co(II) complex.[10a] In the case of **4**, even though each axis of the octahedron has a different donor set, the metal ligand bond lengths are rather similar, and hence there is no pronounced axial distortion in this case as opposed to **1**−**3** even though the symmetry is much lower than O_h.

The room temperature magnetic moment for both **2** and **4** matches well with values expected for isolated octahedral Ni(II) centers. HFEPR data together with simulations provided accurate magnitudes and signs for the D parameter, along with the rhombic parameter, E. It was seen that the D values are positive for complexes **1**−**3** which is expected from the structural data that clearly show an axial elongation for these complexes with the tripodal ligands. Within the complexes **1**−**3**, **2** has a higher D value. It is tempting to assign this difference to the unique C−H···π interactions observed within the secondary coordination sphere of **2**, but this is purely speculation.

An LFT parameter fit was seen to reproduce the experimental absorption spectra with reasonable accuracy. However, quantum chemical calculations show that there are more underlying transitions that are not considered in a simple LFT fit. The reduction of symmetry from O_h to C_1 (in **1** and **4**) and C_i (in **2**) leads to the appearance of multiple transitions, albeit only with small oscillator strengths. A Gaussian deconvolution, together with quantum chemical calculations made the assignment of all the nine spin-allowed transitions possible. High-level *ab initio* calculations at the SA-CASSCF/NEVPT2 level of theory gave more insights into the zfs parameters. In particular, the absolute values of the zfs calculated by NEVPT2 for **1** and **2** compare well with experimental values. In addition, theory uncovered the spin−orbit coupling to triplet excited states as the major contribution to the zfs. Ligand field analysis of the *ab initio* results gave insight into chemical bonding. The N^{ta} atoms proved to be better σ-donors than the N^{am} atoms, which compares well with the bond length analysis of the X-ray structures.

CONCLUSIONS

We have reported here on the synthesis and characterization of Ni(II) complexes with "click" derived triazole ligands, one of which is new: the tripodal tdta. For complexes **1**−**3** an axially distorted octahedral coordination environment is observed around the Ni(II) center that reduces their local symmetry from an ideal O_h to D_{2h} and further to C_1 and C_i. In the case of **4**, which contains bidentate ligands, the triazole N atoms are seen to bind more strongly to the Ni(II) center compared to the pyridine N donors. A comprehensive HFEPR study together with simulations delivered precise zfs parameters from which it can be seen that the magnitude of D for the complexes **1**−**3** is larger than that for **4**, a fact that correlates with the axial structural distortion of **1**−**3**. LFT and *ab initio* calculations at the SA-CASSCF and NEVPT2 levels of theory allowed us to interpret the absorption spectra and extract ligand field parameters. Quantum chemical calculations are in line with the experimental zfs parameters and provided insight into their origin. Furthermore, ligand field analysis of the *ab initio* results allowed distinguishing between the different σ-donating properties of the different nitrogen donor atoms.

To the best of our knowledge, this is the first time that such comprehensive structural, magnetic, HFEPR, LFT, and quantum calculations have been carried out on six-coordinate Ni(II) complexes with $N_4N'_2$ or $N_3N'_3$ donor sets. The results show that structural and hence electronic differences can arise despite the donating atoms being similar. Our studies also highlight the continuing versatility of "click" derived ligands in coordination chemistry and establish the combination of HFEPR and quantum chemical calculations as an extremely powerful tool for elucidating the electronic structure of metal complexes bearing more than one unpaired electron.

EXPERIMENTAL SECTION

Materials and General Methods. All chemicals were used as received unless otherwise mentioned. The ligands tbta and tpta were synthesized according to reported procedures.[18] Elemental analyses were performed with a Perkin-Elmer Analyzer 240. ^{1}H NMR spectra were recorded at 250.13 MHz on a Bruker AC250 instrument. Mass spectrometry experiments were carried out on a Bruker Daltronics Mictrotof-Q mass spectrometer.

Magnetic Susceptibility Measurements. Temperature-dependent magnetic susceptibility measurements were carried out with a Quantum-Design MPMS-XL-5 SQUID magnetometer equipped with a 5 T magnet in the range from 295 to 2.0 K at a magnetic field of 0.5 T. The powdered sample was contained in a gel bucket and fixed in a nonmagnetic sample holder. Each raw data file for the measured magnetic moment was corrected for the diamagnetic contribution of the sample holder and the gel bucket. The molar susceptibility data were corrected for the diamagnetic contribution. Magnetic properties were simulated using the *julX* program (E. Bill, Max Planck Institute for Chemical Energy Conversion, Mülheim/Ruhr, Germany) using the following spin Hamiltonian:

$$\hat{H} = D\left(\hat{S}_z^2 - \frac{1}{3}S(S+1)\right) + g\mu_B\vec{B}\vec{S} \qquad (2)$$

dx.doi.org/10.1021/ic3026123 | Inorg. Chem. 2013, 52, 6880−6892

Temperature-independent paramagnetism (TIP) was included according to $\chi_{calc} = \chi + TIP$ (50×10^{-6} cm^3 mol^{-1} and 150×10^{-6} cm^3 mol^{-1} for **2** and **4**, respectively).

HFEPR Spectroscopy. HFEPR spectra were recorded using the Electron Magnetic Resonance (EMR) Facility at the National High Magnetic Field Laboratory (NHMFL, Tallahassee, FL) using a single-pass transmission homodyne spectrometer. The spectrometer employs a Virginia Diodes (Charlottesville, VA) source operating at a base frequency of 12−14 GHz and multiplied by a cascade of multipliers in conjunction with a 15/17 T superconducting magnet. Detection was provided with an InSb hot-electron bolometer (QMC Ltd., Cardiff, U.K.). The magnetic field was modulated at 50 kHz. A Stanford Research Systems SR830 lock-in amplifier converted the modulated signal to dc voltage. Low temperature was provided by an Oxford Instruments (Oxford, U.K.) continuous flow cryostat with temperature controller (see ref 27 for more details). The typical sample amount was 40−100 mg. All the investigated complexes yielded spectra recognizable as $S = 1$ powder patterns. These spectra were analyzed by simultaneously fitting the parameters of the standard spin Hamiltonian:

$$\mathcal{H} = \beta_e B \cdot g \cdot \hat{S} + D[\hat{S}_z^2 - S(S+1)/3] + E[\hat{S}_x^2 - \hat{S}_y^2] \quad (3)$$

to the complete two-dimensional (field vs frequency) map of turning points, following the principles of tunable-frequency EPR.[19] The sign of zfs was obtained by simulating single-frequency spectra using software (program SPIN) available from A. Ozarowski.

Quantum Chemical Calculations. The program package ORCA 2.9.1[28] was used for all calculations. The coordinates from X-ray structures of **2** and **4** were used without modification. To generate a structural model for **1**, the X-ray structure of **1′** was subjected to a geometry optimization with the BP86 functional.[29] In all calculations, triple-ζ valence quality basis sets (def2-TZVP) were used for all atoms[30] along with empirical van der Waals corrections for the nonbonding interactions.[31] Convergence criteria for the geometry optimization were set to default values and "tight" convergence criteria were used for the SCF procedure. For single point calculations (DFT and unrestricted Hartree−Fock), a combination of the resolution of the identity and the "chain of spheres exchange" algorithms (RIJCOSX) was employed[32,33] with matching auxiliary basis sets.[29,34] The environmental effect were included using the conductor-like screening model (COSMO).[35] The active space of the CASSCF calculations consisted of the 5 metal-based d-orbitals leading to an active space with eight electrons in five orbitals [CAS(8,5)]. The state averaged approach was used where all excited triplet states (10 roots) and all excited singlet states (15 roots) were equally weighted. In addition, for the sake of analysis a reduced number of singlet states (five roots) was used. To recover dynamic correlation, multireference N-electron valence perturbation theory of second order (NEVPT2)[17] was employed on top of the state-averaged CASSCF reference wave functions. MOs were visualized via the program Molekel.[36] Spectral deconvolution was achieved with the ORCA subprogram orca_asa.[28]

Synthesis. *tdta.* 2,6-Diisopropylphenylazide (3.5 g, 17.2 mmol), tripropargylamine (500 mg, 3.8 mmol), $CuSO_4 \cdot 5H_2O$ (143 mg, 0.6 mmol), and TBTA (30 mg, 0.06 mmol) were dissolved in *tert*-butanol/H_2O/DCM (50/25/25 mL). Then sodium ascorbate (454 mg, 2.3 mmmol) was added and the mixture stirred for 3 d at 70 °C. Then water (200 mL) was added, and the reaction mixture was extracted with CH_2Cl_2 (3 × 50 mL). The organic phase was separated and washed with an EDTA/ammonia solution (1 M) (3 × 20 mL). Finally, the solution was dried over Na_2SO_4, and the solvent was evaporated. After flash chromatography over silica (CH_2Cl_2:CH_3OH, 98:2) the product was isolated as a white solid (2.11 g) in 75% yield. Anal. Calcd for $C_{45}H_{60}N_{10} \cdot CH_3OH$: C, 71.47; H, 8.34; N, 18.12. Found: C, 71.20; H, 8.32; 18.41. HRMS (ESI) *m/z*: calcd for $C_{45}H_{60}N_{10}Na$ ($[M + Na]^+$), 763.4895; found, 763.4876. ^{1}H NMR (250 MHz, $CDCl_3$): δ 1.13 − 1.16 (m, 36H, CH_3); 2.29 (qt, $^3J_{H-H}$ = 6.8 Hz, 6H, CH); 4.00 (s, 6H, CH_2); 7.28 (d, $^3J_{H-H}$ = 7.8 Hz, 6H, phenyl); 7.48 (t, $^3J_{H-H}$ = 7.9 Hz, 3H, phenyl); 7.98 (s, 3H, 5-triazole-*H*). ^{13}C NMR (62.5 MHz, $CDCl_3$): δ 24.0; 28.4; 47.1; 123.7; 126.9; 130.7; 133.3; 143.4; 145.9.

pyta. 2-Pyridylacetylene (206 mg, 2.0 mmol), 2,6-di-isopropylphenylazide (406 mg, 2.0 mmol), $CuSO_4 \cdot 5H_2O$ (25 mg, 0.1 mmol), sodium ascorbate (79 mg, 0.4 mmol), and TBTA (11 mg, 0.02 mmol) were dissolved in CH_2Cl_2/H_2O/*tert*-BuOH (2.5 mL/2.5 mL/5 mL) and stirred for 3 d at 50 °C. Then water (50 mL) was added, and the reaction mixture was extracted with CH_2Cl_2 (3 × 20 mL). The organic phase was separated and washed with an EDTA/ammonia solution (1 M) (3 × 10 mL). Finally the solution was dried over Na_2SO_4, and the solvent was evaporated. After flash chromatography over silica (CH_2Cl_2:CH_3OH, 99:1) the product was isolated as a white solid (460 mg) in 75% yield. Anal. Calcd for $C_{19}H_{22}N_4$: C, 74.48; H, 7.24; N, 18.29. Found: C, 74.06; H, 7.37; 18.10. HRMS (ESI) *m/z*: calcd for $C_{19}H_{23}N_4$ ($[M + H]^+$), 307.1917; found, 307.1915. ^{1}H NMR (250 MHz, $CDCl_3$): δ 1.15 (d, $^3J_{H-H}$ = 6.8 Hz, 6H, CH_3); 1.17 (d, $^3J_{H-H}$ = 6.8 Hz, 6H, CH_3); 2.35 (septet, $^3J_{H-H}$ = 6.9 Hz, 2H, CH); 7.28 (t, $^3J_{H-H}$ = 7.5 Hz, 1H, pyridyl); 7.32 (d, $^3J_{H-H}$ = 7.9 Hz, 2H, phenyl); 7.51 (t, $^3J_{H-H}$ = 7.8 Hz, 1H, phenyl); 7.84 (t, $^3J_{H-H}$ = 7.7 Hz, 1H, pyridyl); 8.23 (s, 1H, 5-triazole-*H*); 8.32 (d, $^3J_{H-H}$ = 7.9 Hz, 1H, pyridyl); 8.62 (multiplet, 1H, pyridyl). ^{13}C NMR (62.5 MHz, $CDCl_3$): δ 24.2; 24.4; 28.6; 120.7; 123.2; 124.0; 125.0; 131.0; 133.3; 137.1; 146.3; 148.3; 149.7; 150.5.

[Ni(TPTA)$_2$](BF$_4$)$_2$, ***1***. $Ni(BF_4)_2 \cdot 6H_2O$ (70 mg, 0.20 mmol) and TPTA (200 mg, 0.41 mmol) were dissolved in MeOH (5 mL). The solution was refluxed for 1 h. After the solution cooled, the light pink product precipitated. It was filtered, washed with ether, and isolated in 70% yield (170 mg). Anal. Calcd for $C_{54}H_{48}B_2F_8N_{20}Ni$: C, 53.63; H, 4.00; N, 23.16. Found: C, 52.94; H, 4.31; N, 23.01. HRMS (ESI) *m/z*: calcd for $C_{54}H_{48}N_{20}Ni$ ($[M]^{2+}$), 517.1857; found, 517.1747. IR cm^{-1}: 613(s), 654(s), 687(vs), 756(vs), 824(s), 865(s), 955(s), 1056(br), 1194(s), 1250(s), 1359(s), 1439(s), 1467(s), 1502(s), 1597(s), 3160(br).

[Ni(TBTA)$_2$](BF$_4$)$_2$, ***2***. $Ni(BF_4)_2 \cdot 6H_2O$ (70 mg, 0.20 mmol) and TBTA (218 mg, 0.41 mmol) were dissolved in acetonitrile (5 mL). The solution was refluxed for 1 h. After the solution cooled, ether (5 mL) was added and the light pink product was allowed to crystallize. Then it was filtered, washed with ether, and isolated in 87% yield (225 mg). Single crystals suitable for X-ray diffraction were grown by slow diffusion of ether into an acetonitrile solution. Anal. Calcd for $C_{60}H_{60}B_2F_8N_{20}Ni$: C, 55.71; H, 4.68; N, 21.66. Found: C, 55.67; H, 4.72; N, 21.78. HRMS (ESI) *m/z*: calcd for $C_{60}H_{60}N_{20}Ni$ ($[M]^{2+}$), 559.2326; found, 559.2309. IR cm^{-1}: 579(s), 697(s), 718(vs), 756(s), 823(br), 957(s), 1040(br), 1247(s), 1330(s), 1455(s), 1497(s), 3145(br).

[Ni(TDTA)$_2$](BF$_4$)$_2$, ***3***. $Ni(BF_4)_2 \cdot 6H_2O$ (70 mg, 0.20 mmol) and TDTA 303 mg, 0.41 mmol) were dissolved in EtOH (5 mL). The solution was refluxed for 1 h. After the solution cooled, the light pink product precipitated. It was filtered, washed with ether, and isolated in 85% yield (287 mg). Anal. Calcd for $C_{90}H_{120}B_2F_8N_{20}Ni$: C, 63.05; H, 7.06; N, 16.34. Found: C, 62.51; H, 7.15; N, 16.24. HRMS (ESI) *m/z*: calcd for $C_{90}H_{120}N_{20}Ni$ ($[M]^{2+}$), 769.4674; found, 769.4697. IR cm^{-1}: 624(br), 676(s), 708(s), 759(vs), 803(vs), 862(s), 935(s), 993(s), 1054(br), 1179(s), 1254(br), 1364(br), 1386(s), 1473(br), 2964(br).

[Ni(pyta)$_3$](BF$_4$)$_2$, ***4***. $Ni(BF_4)_2 \cdot 6H_2O$ (74 mg, 0.22 mmol) and pyta (200 mg, 0.65 mmol) were dissolved in EtOH (7.5 mL). The solution was refluxed for 1 h. The hot solution was filtered and the filtrate collected. The filtrate evaporated slowly, and the light pink product precipitated. It was filtered, washed with ether, and isolated in 60% yield (151 mg). Single crystals suitable for X-ray diffraction were grown by slow diffusion of ether into an ethanol solution. Anal. Calcd. for $C_{57}H_{66}B_2F_8N_{12}Ni$: C, 59.45; H, 5.78; N, 14.60. Found: C, 59.20; H, 5.80; N, 14.58. HRMS (ESI) *m/z*: calcd for $C_{57}H_{66}N_{12}Ni$ ($[M]^{2+}$) ,488.2438; found, 488.2338. IR cm^{-1}: 569(s), 643(s), 715(s), 761(s), 785(vs), 806(s), 935(s), 982(s), 1057(br), 1277(s), 1329(s), 1366(s), 1388(s), 1454(vs), 1575(s), 1614(s), 2965(br), 3112(br).

X-ray Crystallography. Suitable single crystals of **2** and **4** were selected and mounted onto a thin glass fiber. X-ray intensity data were measured at 150 K on an Oxford Gemini S Ultra diffractometer with the Enhance X-ray Source of Cu Kα radiation (λ = 1.54178 Å) using

dx.doi.org/10.1021/ic3026123 | *Inorg. Chem.* 2013, 52, 6880−6892

the $\omega-\varphi$ scan technique[37] or with a four circle diffractometer P4 (Siemens, Madison WI) at 173 K. Empirical absorption correction was applied using spherical harmonics implemented in SCALE3 ABSPACK scaling algorithm.[38] The structure was solved by direct methods and refined by full-matrix least-squares against F^2 of all data using the SHELXTL program package.[39] Anisotropic thermal factors were assigned to the non-hydrogen atoms, while the positions of the hydrogen atoms were generated geometrically, assigned isotropic thermal parameters, and allowed to ride on their respective parent atoms before the final cycle of least-squares refinement. CCDC-910983 and 910984 contains the supplementary crystallographic data for this paper. These data can be obtained free of charge from the Cambridge Crystallographic Data Centre via www.ccdc.cam.uk/data_request.cif.

■ ASSOCIATED CONTENT

Ⓢ Supporting Information

Experimental and deconvoluted spectra for **1**, **2**, and **4**. Tables of calculated triplet energies for **2** and **4**; calculated D and E values for **1**, **2**, and **4**; ligand field matrices; and AOM parameters extracted from ligand field analysis of the *ab initio* results. This material is available free of charge via the Internet at http://pubs.acs.org.

■ AUTHOR INFORMATION

Corresponding Author

*E-mail: krzystek@magnet.fsu.edu (J.K.), jtelser@roosevelt.edu (J.T.), mihail.atanasov@cec.mpg.de (M.A.), frank.neese@cec.mpg.de (F.N.), biprajit.sarkar@fu-berlin.de (B.S.).

Notes

The authors declare no competing financial interest.

■ ACKNOWLEDGMENTS

We are indebted to the Fonds der Chemischen Industrie (FCI) for financial support of this project (Chemiefondsstipendium for D.S.). Denis Bubrin is kindly acknowledged for the crystal structure determination of **2** and Stephan Hohloch for **1′**. We are thankful to Sebastian Weber for synthetic help. The HFEPR work was done at the National High Magnetic Field Laboratory, which is funded by the NSF through the Cooperative Agreement DMR 1157490, the State of Florida, and the U.S. Department of Energy.

■ REFERENCES

(1) (a) Rostovtsev, V.; Green, L. G.; Fokin, V. V.; Sharpless, K. B. *Angew. Chem., Int. Ed.* **2002**, *41*, 2596. (b) Tornoe, C. V.; Christensen, C.; Meldal, M. *J. Org. Chem.* **2002**, *67*, 3057. (c) Lau, Y. H.; Rutledge, P. J.; Watkinson, M.; Todd, M. H. *Chem. Soc. Rev.* **2011**, *40*, 2848. (d) Hua, Y.; Flood, A. H. *Chem. Soc. Rev.* **2010**, *39*, 1262.

(2) (a) Liang, L.; Astruc, D. *Coord. Chem. Rev.* **2011**, *255*, 2933. (b) Struthers, H.; Mindt, T. L.; Schibli, R. *Dalton Trans.* **2010**, *39*, 675. (c) Crowley, J. D.; McMorran, D. In *Topics in Heterocyclic Chemistry*; Kosmrlj, J., Ed.; Springer: Berlin/Heidelberg, 2012; Vol. *28*, pp 31. (d) Schweinfurth, D.; Deibel, N.; Weisser, F.; Sarkar, B. *Nachr. Chem.* **2011**, *59*, 937. (e) Aromi, G.; Barrios, L. A.; Robeau, O.; Gamez, P. *Coord. Chem. Rev.* **2011**, *255*, 485.

(3) (a) Li, Y.; Huffman, J. C.; Flood, A. H. *Chem. Commun.* **2007**, 2692. (b) Meudtner, R. M.; Ostermeier, M.; Goddard, R.; Limberg, C.; Hecht, S. *Chem.—Eur. J.* **2007**, *13*, 9834. (c) Fletcher, J. T.; Bumgarner, B. J.; Engels, N. D.; Skoglund, D. A. *Organometallics* **2008**, *27*, 5430. (d) Yang, W. W.; Wang, L.; Zhong, Y. W.; Yao, Y. *Organometallics* **2011**, *30*, 2236. (e) Richardson, C.; Fitchett, C. M.; Keene, F. R.; Steel, P. J. *Dalton Trans.* **2008**, 2534. (f) Schulze, B.; Friebe, C.; Hager, M. D.; Winter, A.; Hoogenboom, R.; Goerls, H.; Schubert, U. S. *Dalton Trans.* **2009**, 787. (g) Happ, B.; Friebe, C.; Winter, A.; Hager, M. D.; Hoogenboom, R.; Schubert, U. S. *Chem.—Asian J.* **2009**, *4*, 154.

(4) (a) Swanick, K. N.; Ladouceur, S.; Zysman-Colman, E.; Ding, Z. *Chem. Commun.* **2012**, *48*, 3179. (b) Brown, D. G.; Sanguantrakun, N.; Schulze, B.; Schubert, U. S.; Berlinguette, C. P. *J. Am. Chem. Soc.* **2012**, *134*, 12354. (c) Manbeck, G. F.; Brennessel, W. W.; Eisenberg, R. *Inorg. Chem.* **2011**, *50*, 3431. (d) Mydlak, M.; Bizzarri, C.; Hartmann, D.; Sarfert, W.; Schmid, G.; De Cola, L. *Adv. Funct. Matter* **2010**, *20*, 1812.

(5) (a) Ostermeier, M.; Berlin, M.-A.; Meudtner, R. M.; Demeshko, S.; Meyer, F.; Limberg, C.; Hecht, S. *Chem.—Eur. J.* **2010**, *16*, 10202. (b) Guha, P. M.; Phan, H.; Kinyon, J. S.; Brotherton, W. S.; Sreenath, K.; Simmons, J. T.; Wang, Z.; Clark, R. J.; Dalal, N. S.; Shatruk, M.; Zhu, L. *Inorg. Chem.* **2012**, *51*, 3465.

(6) (a) Maisonial, A.; Serafin, P.; Traikia, M.; Debiton, E.; Théry, V.; Aitken, D. J.; Lemoine, P.; Viossat, B.; Gautier, A. *Eur. J. Inorg. Chem.* **2008**, 298. (b) Chevry, A.; Teyssot, M. L.; Maisonial, A.; Lemoine, P.; Viossat, B.; Traikia, M.; Aitken, D. J.; Alves, G.; Morel, L.; Nauton, L.; Gautier, A. *Eur. J. Inorg. Chem.* **2010**, 3513.

(7) (a) Crowley, J. D.; Bandeen, P. H. *Dalton Trans.* **2010**, *39*, 612. (b) Bai, S.-Q.; Leelasubcharoen, S.; Chen, X.; Koh, L. L.; Juo, J.-L.; Hor, T. S. A. *Cryst. Growth Des.* **2010**, *10*, 1715. (c) Steinmetz, V.; Couty, F.; David, O. R. P. *Chem. Commun.* **2009**, 343. (d) Collason, B.; Paul, N. L.; Mest, Y. L.; Reinaud, O. *J. Am. Chem. Soc.* **2010**, *132*, 4393. (e) Aucagne, V.; Berna, J.; Crowley, J. D.; Goldup, S. M.; Hanni, K. D.; Leigh, D. A.; Lusby, P. J.; Ronaldson, V. E.; Slawin, A. M. Z.; Viterisi, A.; Walker, D. B. *J. Am. Chem. Soc.* **2007**, *129*, 11950. (f) Clough, M. C.; Zeits, P. D.; Bhuvanesh, N.; Gladysz, J. A. *Organometallics* **2012**, *31*, 5231. (g) Urankar, D.; Pevec, A.; Kosmrlj, J. *Cryst. Growth Des.* **2010**, *10*, 4920. (h) Younes, A. H.; Clark, R. J.; Zhu, L. *Supramol. Chem.* **2012**, *24*, 696. (i) Crowley, J. D.; Gavey, E. L. *Dalton Trans.* **2010**, *39*, 4035. (j) Scott, S. O.; Gavey, E. L.; Lind, S. L.; Gordon, K. C.; Crowley, J. D. *Dalton Trans.* **2011**, *40*, 12117. (k) Stevenson, K. A.; Melan, C. F. C.; Fleischel, O.; Wang, R.; Petitjean, A. *Cryst. Growth Des.* **2012**, *12*, 5169. (l) White, N. G.; Beer, P. D. *Supramol. Chem.* **2012**, *24*, 473.

(8) (a) Gu, S.; Xu, H.; Zhang, N.; Chen, Y. *Chem. Asian. J.* **2010**, *5*, 1677. (b) Cambeiro, X. C.; Pericas, M. A. *Adv. Synth. Cat.* **2011**, *353*, 113. (c) Lalrempuia, R.; McDaniel, N. D.; Müller-Bunz, H.; Bernhard, S.; Albrecht, M. *Angew. Chem., Int. Ed.* **2010**, *49*, 9765. (d) Kilpin, K. J.; Paul, U. S. D.; Lee, A.-L.; Crowley, J. D. *Chem. Commun.* **2011**, *47*, 328. (e) Saravanakumar, R.; Ramkumar, V.; Sankararaman, S. *Organometallics* **2011**, *30*, 1689. (f) Hua, C.; Vuong, K. Q.; Bhadbhade, M.; Messerle, B. A. *Organometallics* **2012**, *31*, 1790.

(9) (a) Schweinfurth, D.; Pattacini, R.; Strobel, S.; Sarkar, B. *Dalton Trans.* **2009**, 9291. (b) Schweinfurth, D.; Strobel, S.; Sarkar, B. *Inorg. Chim. Acta* **2011**, *374*, 253. (c) Hohloch, S.; Su, C.-Y.; Sarkar, B. *Eur. J. Inorg. Chem.* **2011**, 3067.

(10) (a) Schweinfurth, D.; Weisser, F.; Bubrin, D.; Bogani, L.; Sarkar, B. *Inorg. Chem.* **2011**, *50*, 6114. (b) Schweinfurth, D.; Demeshko, S.; Khusniyarov, M. M.; Dechert, S.; Gurram, V.; Buchmeiser, M. R.; Meyer, F.; Sarkar, B. *Inorg. Chem.* **2012**, *51*, 7592. (c) Schweinfurth, D.; Su, C.-Y.; Wei, S.-C.; Braunstein, P.; Sarkar, B. *Dalton Trans.* **2012**, *41*, 12984.

(11) (a) Krzystek, J.; Ozarowski, A.; Telser, J. *Coord. Chem. Rev.* **2006**, *250*, 2308. (b) Telser, J.; Ozarowski, A.; Krzystek, J. *Specialist Periodical Reviews of the Royal Chemical Society: Electron Paramagnetic Resonance* **2013**, *23*, 209.

(12) (a) Boča, R. *Coord. Chem. Rev.* **2004**, *248*, 757. (b) Titiš, J.; Boča, R. *Inorg. Chem.* **2010**, *49*, 3971.

(13) Gispert, J. R. *Coordination Chemistry*: Wiley-VCH: Weinheim, 2008.

(14) (a) van Dam, P. J.; Klaassen, A. A.K.; Reijerse, E. J.; Hagen, W. R. *J. Magn. Reson.* **1998**, *130*, 140. (b) Pardi, L.; Hassan, A. K.; Hulsbergen, F. B.; Reedjik, J.; Spek, A. L.; Brunel, L. C. *Inorg. Chem.* **2000**, *39*, 159. (c) Collison, D.; Helliwell, M.; Jones, V. M.; Mabbs, F. E.; McInnes, E. J. L.; Riedi, P. C.; Smith, G. M.; Pritchard, R. G.; Cross, W. I. *J. Chem. Soc. Faraday Trans.* **1998**, *94*, 3019. (d) Krzystek, J.; Park, J. H.; Meisel, M. W.; Hitchman, M. A.; Stratemeier, H.;

Brunel, L. C.; Telser, J. *Inorg. Chem.* **2002**, *41*, 4478. (e) Rebilly, J. N.; Charron, G.; Riviere, E.; Guillot, R.; Barra, A. L.; Serrano, M. D.; van Slageren, J.; Mallah, T. *Chem.—Eur. J.* **2008**, *14*, 1169. (f) Mrozinski, J.; Skorupa, A.; Pochaba, A.; Dromzee, Y.; Verdaguer, M.; Goovaerts, E.; Varcammen, H.; Korybut-Daszkiewicz, B. *J. Mol. Struct.* **2001**, *559*, 107. (g) Yang, E. C.; Kirman, C.; Lawrence, J.; Zakharov, L. N.; Rheingold, A. L.; Hill, S.; Hendrickson, D. N. *Inorg. Chem.* **2005**, *44*, 3827. (h) Rogez, G.; Rebilly, J. N.; Barra, A. L.; Sorace, L.; Blondin, G.; Kirchner, N.; Duran, M.; van Slageren, J.; Parsons, S.; Ricard, L.; Marvilliers, A.; Mallah, T. *Angew. Chem., Int. Ed.* **2005**, *44*, 1876. (i) Dobrzynska, D.; Jerzykiewicz, L. B.; Duczmal, M.; Wojciechowska, A.; Jablonska, K.; Palus, J.; Ozarowski, A. *Inorg. Chem.* **2006**, *45*, 10479. (j) Desrochers, P. J.; Telser, J.; Zvyagin, S. A.; Ozarowski, A.; Krzystek, J.; Vicic, D. A. *Inorg. Chem.* **2006**, *45*, 8930. (k) Wojciechowska, A.; Daszkiewicz, M.; Staszak, Z.; Trusz-Zdybek, A.; Bienko, A.; Ozarowski, A. *Inorg. Chem.* **2011**, *50*, 11532. (l) Charron, G.; Bellot, F.; Cisnetti, F.; Pelosi, G.; Rebilly, J. N.; Riviere, E.; Barra, A. L.; Mallah, T.; Policar, C. *Chem.—Eur. J.* **2007**, *13*, 2774. (m) Maganas, D.; Krzystek, J.; Ferentinos, E.; Whyte, A. M.; Robertson, N.; Psycharis, V.; Terzis, A.; Neese, F.; Kyritsis, P. *Inorg. Chem.* **2012**, *51*, 7218.

(15) (a) Atanasov, M.; Ganyushin, D.; Sivalingam, K.; Neese, F. *Struct. Bonding (Berlin, Ger.)* **2012**, *143*, 149. (b) Atanasov, M.; Ganyushin, D.; Pantazis, D. A.; Sivalingam, K.; Neese, F. *Inorg. Chem.* **2011**, *50*, 7640. (c) Atanasov, M.; Zadrozny, J. M.; Long, J. R.; Neese, F. *Chem. Sci.* **2013**, *4*, 139. (d) Atanasov, M.; Comba, P.; Helmle, S.; Müller, D.; Neese, F. *Inorg. Chem.* **2012**, *51*, 12324. (e) Neese, F. *WIREs Comput. Mol. Sci.* **2012**, *2*, 73.

(16) Malmqvist, P.-Å; Roos, B. O. *Chem. Phys. Lett.* **1989**, *155*, 189.

(17) (a) Angeli, C.; Cimiraglia, R.; Malrieu, J.-P. *Chem. Phys. Lett.* **2001**, *350*, 297. (b) Angeli, C.; Cimiraglia, R.; Evangelisti, S.; Leininger, T.; Malrieu, J.-P. *J. Chem. Phys.* **2001**, *114*, 10252. (c) Angeli, C.; Cimiraglia, R.; Malrieu, J.-P. *J. Chem. Phys.* **2002**, *117*, 9138. (d) Borini, S.; Cestari, M.; Cimiraglia, R. J. *J. Chem. Phys.* **2004**, *121*, 4043. (e) Angeli, C.; Bories, B.; Cavallini, A.; Cimiraglia, R. *J. Chem. Phys.* **2006**, *124*, 54108.

(18) Hein, J. E.; Krasnova, L. B.; Iwasaki, M.; Fokin, V. V. *Org. Synth.* **2011**, *88*, 238.

(19) Krzystek, J.; Zvyagin, S. A.; Ozarowski, A.; Trofimenko, S.; Telser, J. *J. Magn. Reson.* **2006**, *178*, 174.

(20) Ballhausen, C. J. In *Introduction to Ligand Field Theory*; McGraw-Hill: New York, 1962; pp 99−103.

(21) (a) Lovecchio, F. V.; Gore, E. S.; Busch, D. H. *J. Am. Chem. Soc.* **1974**, *96*, 3109. (b) Martin, L. Y.; Sperati, C. R.; Busch, D. H. *J. Am. Chem. Soc.* **1977**, *99*, 2968.

(22) Bendix, J.; Brorson, M.; Schaeffer, C. E. *Inorg. Chem.* **1993**, *32*, 2838.

(23) (a) Liakos, D. G.; Ganyushin, D.; Neese, F. *Inorg. Chem.* **2009**, *48*, 10572. (b) Duboc, C.; Ganyushin, D.; Sivalingam, K.; Collomb, M.-N.; Neese, F. *J. Phys. Chem. A* **2010**, *114*, 10750. (c) Maganas, D.; Sottini, S.; Kyritsis, P.; Groenen, E. J. J.; Neese, F. *Inorg. Chem.* **2011**, *50*, 8741. (d) Domingo, A.; Carvajal, M. A.; de Graaf, C.; Sivalingam, K.; Neese, F.; Angeli, C. *Theor. Chem. Acc.* **2012**, *131:1264*, 1.

(24) Bencini, A.; Benelli, C.; Gatteschi, D. *Coord. Chem. Rev.* **1984**, *60*, 131.

(25) Jørgensen, C. K.; Pappalardo, R.; Schmidtke, H.-H. *J. Chem. Phys.* **1963**, *39*, 1422.

(26) Schäffer, C. E.; Jørgensen, C. K. *Mol. Phys.* **1965**, *9*, 401.

(27) Hassan, A. K.; Pardi, L. A.; Krzystek, J.; Sienkiewicz, A.; Goy, P.; Rohrer, M.; Brunel, L. C. *J. Magn. Reson.* **2000**, *142*, 300−312.

(28) Neese, F. with contributions from Becker, U.; Ganyushin, G.; Hansen, A.; Izsak, R.; Liakos, D. G.; Kollmar, C.; Kossmann, S.; Pantazis, D. A.; Petrenko, T.; Reimann, C.; Riplinger, C.; Roemelt, M.; Sandhöfer, B.; Schapiro, I.; Sivalingam, K.; Wennmohs, F.; Wezisla, B. and contributions from our collaborators: Kállay, M.; Grimme, S.; Valeev, E. *ORCA - An ab initio, DFT and semiempirical SCF-MO package*, Version 2.9.1; Mülheim a.d.R. The binaries of ORCA are available free of charge for academic users for a variety of platforms.

(29) Becke, A. D. *Phys. Rev.* **1988**, *A38*, 3098. Perdew, J. P. *Phys. Rev.* **1986**, *B33*, 8822.

(30) Weigend, F.; Ahlrichs, R. *Phys. Chem. Chem. Phys.* **2005**, *7*, 3297.

(31) Grimme, S.; Antony, J.; Ehrlich, S.; Krieg, H. *J. Chem. Phys.* **2010**, *132*, 154104.

(32) Neese, F.; Wennmohs, F.; Hansen, A.; Becker, U. *Chem. Phys.* **2009**, *356*, 98.

(33) Neese, F. *J. Comput. Chem.* **2003**, *24*, 1740.

(34) (a) Eichkorn, K.; TGreutler, O.; Ohm, H.; Haser, M.; Ahlrichs, R. *Chem. Phys. Lett.* **1995**, *242*, 652. (b) Eichkorn, K.; Weigend, F.; Treutler, O.; Ahlreichs, R. *Theor. Chem. Acc.* **1997**, *97*, 119.

(35) Klamt, A.; Schüürmann, G. *J. Chem. Soc., Perkin Trans. 2* **1993**, 799.

(36) Portmann, S. *Molekel*, version 5.4.0.8; CSCS/UNI Geneva: Geneva, Switzerland, 2009.

(37) *CrysAlis CCD*, version 1.171.31.7; Oxford Diffraction Ltd.

(38) *CrysAlis RED*, version 1.171.31.7; Oxford Diffraction Ltd.

(39) *SHELXTL*, version 5.10; Bruker Analytical X-ray Systems: Madison, WI, 1998.